Flexural Analysis and Design of Textile Reinforced Concrete*

Chote Soranakom[1] and Barzin Mobasher[2]

Summary: A model is presented to use normalized multi-linear tension and compression material characteristics of strain-hardening textile reinforced concrete and derive closed form expressions for predicting moment-curvature capacity. A set of design equations are derived and simplified for use in spreadsheet based applications. The model is applicable for both strain-softening and strain-hardening materials. The predictability of the simplified model is checked by model calibration and development of design charts for moment capacity and stress developed throughout the cross section of a flexural member. Model is calibrated by predicting the results of Alkali Resistant Glass and Polyethylene fabrics. A case for the flexural design of Glass Fiber Reinforced Concrete (GFRC) specimen as a simply supported beam subjected to distributed load is used to demonstrate the design procedure.

1 Introduction

Recent interest in the area of Textile Reinforced Concrete (TRC) has led to the development of novel cement based materials with a significant degree of strength, ductility, and versatility. These materials that are as much as an order of magnitude higher in strength and two orders of magnitude higher in ductility than fiber reinforced concrete (FRC), have been developed using innovative fabrics, matrices and manufacturing processes such as computer controlled closed loop pultrusion and filament winding. A variety of fiber and fabric systems such as Alkali resistant (AR) glass fibers, polypropelene (PE), polyethylene (PE), and Poly Vinyl Alcohol (PVA) have been utilized [1,2]. Mechanical properties of the composites measured using uniaxial tensile, flexural, and shear tests indicate that the tensile strength as high as 25 MPa, and strain capacity of 1-8%. The fracture toughness as compared to the conventional FRC materials is increased by as much as two orders of magnitude. The dominant toughening mechanisms in these systems are attributed to matrix cracking, ply delamination, and crack deflection mechanisms as studied by means of fluorescent microscopy, scanning electron microscopy. TRC materials currently compete with a range of other propriety prod-

* This is a peer-reviewed paper. Online available: urn:nbn:de:bsz:14-ds-1244046537373-61938
[1] Post Doctoral Research Associate, Dept. of Civil & Env. Eng., Arizona State University, USA
[2] Professor, Dept. of Civil & Env. Eng., Arizona State University, USA

ucts under trademark CARDIFRC® [3] and Ductal® [4], and ECC [5]. The difference however is that the work conducted in the area of TRC materials is conducted and published in open literature thus resulting in a significant number of publications that have propelled this area to a new stage.

Strain hardening materials are well suited for applications that eliminate conventional reinforcement or for the structures in seismic regions where high ductility is desired. In addition, these materials offer fatigue and impact resistance and are attractive for use in industrial structures, highways, bridges, earthquake, hurricane, and high wind loading conditions. The design and implementation of these systems requires one to acknowledge and use the strain-hardening response that is attributed to multiple cracking during a tension test. The post-crack response that exceeds the first crack stress over a large strain range is modeled using a reduced stiffness parameter. Unlike FRC that fracture localization occurs immediately after the first crack is formed, propagation of initial crack in strain hardening composites is resisted by fiber bridging mechanism. Since a substantial amount of energy is required to further extend existing cracks, secondary cracks form. Single crack localization is therefore shifted to multiple distributed cracking mechanisms, leading to macroscopic pseudo-strain hardening behaviors. Classes of strain-softening and hardening FRC are discussed by Naaman and Reinhardt [6].

In order to facilitate the potential use of these materials, fundamental approaches for tensile and flexural design are needed. This paper addresses methods to predict moment-rotation capacity integrated with a general template for predicting load deformation performance is presented. Two examples of analysis and design of various structural systems are used to demonstrate the calculation steps.

2 Simplified Strain-Hardening Fiber Reinforced Concrete Model

A general strain hardening tensile, and a elastic perfectly plastic compression model as derived by Soranakom and Mobasher [7] and shown in Fig. 1 is used. Tensile response is defined by tensile stiffness, E, first crack tensile strain ε_{cr}, cracking tensile strength, $\sigma_{cr} = E\varepsilon_{cr}$, post crack modulus E_{cr} and ultimate tensile capacity, ε_{tm}. The post peak tensile capacity, or the softening range is shown as a constant stress level $\mu E\varepsilon_{cr}$. The compression response is defined by the compressive strength σ_{cy} defined as $\omega\gamma E\varepsilon_{cr}$. In order to simplify material characteristics of strain-hardening FRC, and yet obtain closed form design equation generation several assumptions are made. Equations can furthermore be simplified to idealized bilinear tension and elastic compression models as shown in Fig. 2(a)&(b) by ignoring the post-peak ranges in both tension and compression. In order to reduce the complexity of material response to the useable range, one has to disregard the post-peak tensile response and plasticity in the compression region. It has been shown that the difference in compressive and tensile modulus has negligible effect to the ultimate moment capacity [7]. By defining all parameters as normalized with respect to minimum number of variables, closed form derivations are ob-

tained. Applied tensile and compressive strains at bottom and top fibers, β, and λ are defined as

$$\beta = \frac{\varepsilon_t}{\varepsilon_{cr}},\ \lambda = \frac{\varepsilon_c}{\varepsilon_{cr}} \qquad (1)$$

Material parameters required for the simplified models are summarized as follows. Parameters, α, μ, η, ω, are defined respectively as representing normalized, tensile strain at peak strength, post-crack modulus, compressive yield strain:

$$\alpha = \frac{\varepsilon_{tm}}{\varepsilon_{cr}},\ \eta = \frac{E_{cr}}{E},\ \omega = \frac{\sigma_{cy}}{E\varepsilon_{cr}} = \frac{\sigma_{cy}}{\sigma_{cr}} \qquad (2)$$

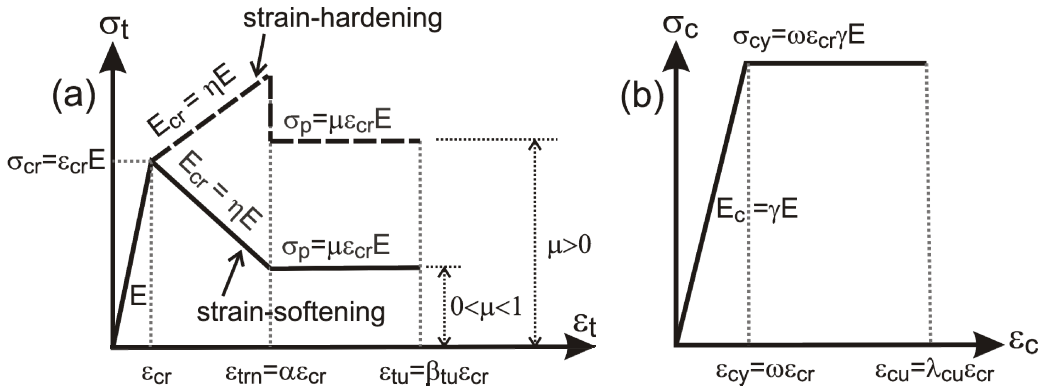

Fig. 1: Full option material models for both strain-hardening and strain-softening FRC: (a) tension model and (b) compression model;

For typical strain-hardening FRC, the compressive strength is several times higher than the tensile strength. Thus, the flexural capacity is controlled by the weaker tension and the compressive stress is normally low in the elastic range. For this reason, the elastic compression model [Fig. 2(b)] is used. For the development of design equations, the compressive stress developed in a beam section is limited to the yield compressive stress $\sigma_{cy} = 0.85f_c'$ at compressive yield strain ε_{cy}, where f_c' is the uniaxial compressive strength.

3 Derivation of Moment Capacity

Moment capacity of a beam section according to the imposed tensile strain at the bottom fiber ($\varepsilon_t = \beta\varepsilon_{cr}$) can be derived based on the assumed linear strain distribution as shown in Fig. 2(a). By using material models described in Fig. 1(a)&(b), the corresponding stress diagram is obtained as shown in Fig. 2(b) in which the stress distribution is subdivided into a compression zone 1, tension zone 1 and 2. Force components and their centroidal distance to the neutral axis in each zone can be expressed as:

$$\frac{F_{c1}}{bh\sigma_{cr}} = \frac{\beta\gamma k^2}{2(1-k)};\ \frac{y_{c1}}{h} = \frac{2}{3}k \tag{3}$$

$$\frac{F_{t1}}{bh\sigma_{cr}} = \frac{(1-k)}{2\beta};\quad \frac{y_{t1}}{h} = \frac{2}{3}\frac{(1-k)}{\beta} \tag{4}$$

$$\frac{F_{t2}}{bh\sigma_{cr}} = \frac{(1-k)(\beta-1)(\eta\beta-\eta+2)}{2\beta};\quad \frac{y_{t2}}{h} = \frac{2\eta\beta^2-\eta\beta-\eta+3\beta+3}{3\beta(\eta\beta-\eta+2)}(1-k) \tag{5}$$

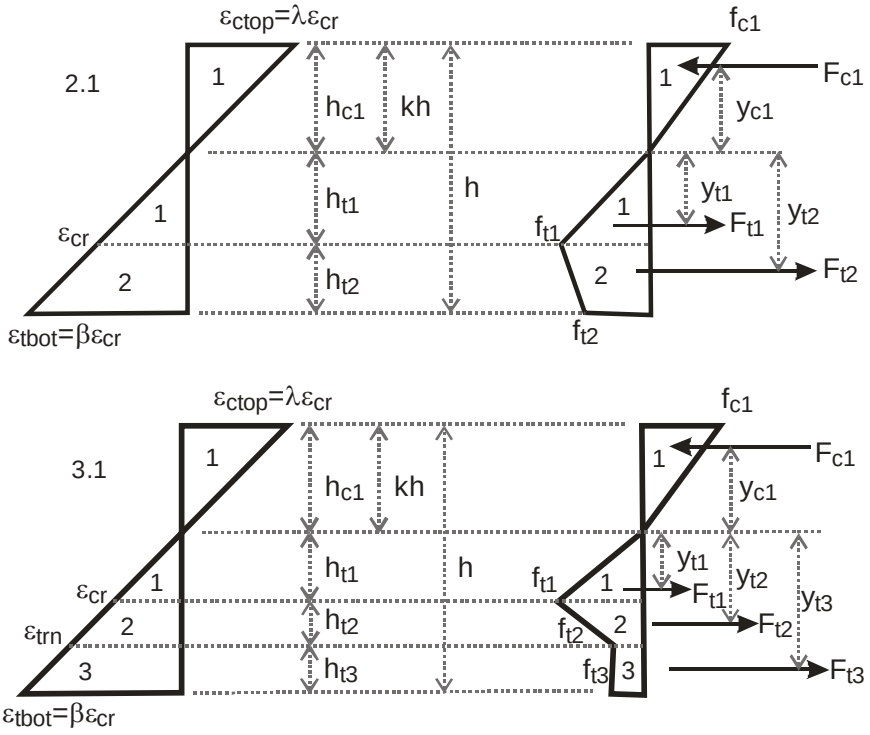

Fig. 2: Strain and stress diagrams at the post crack stage (Ranges 2.1, and 3.1 Table 1), (a) strain distribution; and (b) stress distribution

where F and y are the force and its centroid, respectively; subscripts *c1,t1,t2* designate compression zone 1, tension zone 1 and 2, respectively; b and h are the width and the height of the beam, respectively. In Zone 2.1, the post peak tensile response, $\mu E\varepsilon_{cr}$, does not play a role, and the neutral axis parameter k is found by solving the equilibrium of net internal forces equal to zero, $F_{c1} + F_{t1} + F_{t2} = 0$.

$$k = \frac{C_1 - \sqrt{\beta^2 C_1}}{C_1 - \beta^2};\ \text{where}\ C_1 = \eta\left(\beta^2 - 2\beta + 1\right) + 2\beta - 1 \tag{6}$$

The nominal moment capacity M_n is obtained by taking the first moment of force about the neutral axis, $M_n = F_{c1}y_{c1} + F_{t1}y_{t1} + F_{t2}y_{t2}$, and it is expressed as a product of the normalized nominal moment m_n and the cracking moment M_{cr} (for γ=1) as follows:

$$M_n = m_n M_{cr} \quad , \quad M_{cr} = \frac{\sigma_{cr} b h^2}{6} \tag{7}$$

$$m_n = C_2 \frac{k^2 - 2k + 1}{\beta^2} + \frac{2\beta k^3}{1-k}; \text{ where } C_2 = C_1 + 2C_1\beta - \beta^2 \tag{8}$$

If the full stress strain response is desired, then the location of Neutral axis and moment capacity are obtained under the definitions provided in Table 1. In zone 3.1 and 3.2, the equations listed in Table 1 can be simplified and used similar to equations 6, 7 and 8. In this table the derivations of all potential combinations for the interaction of tensile and compressive response are presented. Note that depending on the relationship among material parameters, any of the zones 2.a, and 2.b, or 3.a, and 3.b are potentially possible.

Analysis of these equations indicates that the contribution of fibers is mostly apparent in the post cracking tensile region, where the response continues to increase after cracking [Fig. 1(a)]. The post-crack modulus E_{cr} is relatively flat with values of η= 0.00-0.4 for a majority of cement composites. The tensile strain at peak strength ε_{peak} is relatively large compared to the cracking tensile strain ε_{cr} and may be as high as α = 100 for polymeric based fiber systems. These unique characteristics cause the flexural strength to increase after cracking. If the post-peak tensile strength is ignored in the typical strain-hardening FRC, the flexural strength reaches its maximum at the maximum tensile strength. Furthermore the effect of post crack tensile response parameter μ can be ignored for a simplified analysis. In the most simplistic way, one needs to determine two parameters in terms of post crack stiffness η, and post crack ultimate strain capacity α, to estimate the maximum moment capacity for the design purposes.

According to bilinear tension and elastic compression models shown in Fig. 1(a)&(b), the maximum moment capacity is obtained when the normalized tensile strain at the bottom fiber ($\beta = \varepsilon_t/\varepsilon_{cr}$) reaches the tensile strain at peak strength ($\alpha = \varepsilon_{tm}/\varepsilon_{cr}$). The simplified equations (8) - (10) for moment capacity are applicable for the compressive stress in elastic region only. The elastic condition must be checked by computing the normalized compressive strain developed at the top fiber λ and compare it to the normalized yield compressive strain ω. The general solutions for all the cases are presented in Table 1. Using the strain diagram in Fig. 2(a), one can obtain the relationship between the top compressive strain and bottom tensile strain as follow:

$$\frac{\varepsilon_c}{kh} = \frac{\varepsilon_t}{(1-k)h} \tag{9}$$

By substituting $\varepsilon_c = \lambda\varepsilon_{cr}$ and $\varepsilon_t = \beta\varepsilon_{cr}$ in Eq.(9), then limit the maximum compressive strain to the yield compressive strain $\varepsilon_{cy} = \omega\varepsilon_{cr}$. Finally, the condition expressed in a normalized form is:

$$\lambda = \frac{k}{1-k}\beta \quad \leq \quad \omega \tag{10}$$

The case represented by case 2.1 of Table 1, where the tensile behavior is elastic-plastic while the compressive behavior is still elastic is studied next. Equations for other cases can also be developed. The general solution presented in Table 1 can be simplified as follows. The location of Neutral axis represented as a function of applied tensile strain β is represented as:

$$k = \frac{\sqrt{A}}{\sqrt{A} + \beta\sqrt{\gamma}} \qquad A = \eta(\beta^2 + 1 - 2\beta) + 2\beta - 1 \tag{11}$$

This equation can be easily simplified by assuming equal tension and compression stiffness (γ=1). Furthermore, for elastic perfectly plastic tension materials (η=0) the equation reduces to:

$$k = \frac{\sqrt{2\beta - 1}}{\sqrt{2\beta - 1} + \beta} \tag{12}$$

Table 2 presents the case of (γ=1), for different values of post-crack stiffness η = 0.5, 0.2, 0.1, 0.05, 0.01, and 0.001. Note that the neutral axis is a function β and can be used in calculation of the moment, or the moment curvature relationship. These general response are shown in Figures 4a and 4b and show that with an increase in applied tensile strain, the neutral axis compression zone decreases, however this decrease is a function of post crack tensile stiffness factor. The moment curvature relationship in this range in ascending, however, its rate is a function of the post crack tensile stiffness. The parameter based fit equations in the third and fourth column are obtained by curve fitting the simulated response from the closed form derivations and are applicable within 1% accuracy of the closed form results. Using these equations, one can generate the moment capacity and moment-curvature response for any cross section using basic tensile material parameters in the 2.1 range as defined in Table 2.

4 Analysis - Prediction of Load Deflection Response of Fabric Cement Composites

Two types of fabric systems are discussed including bonded Alkali Resistant (AR) glass, and woven polyethylene mesh. AR glass Fabric reinforced cement composites were manufactured using a cement paste with a water to cement ratio of 0.45, and AR glass fabrics manufactured by Saint-Gobain Technical Fabrics Inc. The grid size was 25.4x25.4 mm with 2 yarns in each the longitudinal and transverse directions. Each yarn consisted of 1579 filaments, each 19 microns in diameter. Two layers of fabric were placed at the top and bottom of the specimens to provide reinforcement in each direction: $V_L = V_T$ = 0.70%. Figure 4.a represents the tensile stress stain response of the AR Glass sample. The initial response is linear elastic up to about 2 MPa. After cracking the load is transferred to the fabric layers. Subsequent cracking results in formation of parallel cracks [8][9]. As multiple cracking takes place, the stiffness of the sample significantly drops while the crack spacing continuously decreases up to about 20 mm and reaches saturation crack spacing at this level. The saturation of crack spacing correlates to overall strain levels corresponding to 1.5%. The reduced stiffness of the sample in the post crack region is clearly shown. A similar behavior is also obtained from the Polyethylene fabric composite samples. The stress strain and crack spacing response is shown in Figure 4.b. Note that the slope in the post crack phase is significantly lower than the AR glass composites, however the strain capacity is higher and the crack spacing is much smaller than AR Glass composites.

Table 1: Neutral axis, moment, and moment-curvature of a material with $\gamma = 1$ $\eta = 0.0001$- 0.5.

η	A, $(k = \frac{\sqrt{A}}{\sqrt{A}+\beta})$	$M'(k)$	$M'(\varphi)$
0.5	$0.5(\beta^2+1-2\beta)+2\beta-1$	$-0.773+0.108x10^{-1}k^{-6}$	$0.507+0.686\varphi$
0.2	$0.2(\beta^2+1-2\beta)+2\beta-1$	$0.654+0.516x10^{-2}k^{-6}$	$1.105+0.383\varphi$
0.1	$0.1(\beta^2+1-2\beta)+2\beta-1$	$1.276+0.289x10^{-2}k^{-6}$	$1.461+.234\varphi$
0.05	$0.05(\beta^2+1-2\beta)+2\beta-1$	$1.645+.1632x10^{-2}k^{-6}$	$1.720+.1401\varphi$
0.01	$0.01(\beta^2+1-2\beta)+2\beta-1$	$0.852+0.456\,k^{-1}$	$1.342+0.371\sqrt{\varphi}$
0.0001	$0.0001(\beta^2+1-2\beta)+2\beta-1$	$3.177-3.068\,k$	$3.021-2.047/\sqrt{\varphi}$

Table 2: Neutral axis parameter k, normalized moment m and normalized curvature ϕ for each stage of normalized tensile strain at bottom fiber (β)

Stage	Parameters	K	$m = M/M_{cr}$	$\phi = \Phi/\Phi_{cr}$
1	$0 < \beta \le 1$	$k_1 = \begin{cases} \frac{1}{2} & \text{for } \gamma = 1 \\ \frac{-1+\sqrt{\gamma}}{-1+\gamma} & \text{for } \gamma \ne 1 \end{cases}$	$m_1 = \frac{2\beta\left[(\gamma-1)k_1^3 + 3k_1^2 - 3k_1 + 1\right]}{1-k_1}$	$\phi'_1 = \frac{\beta}{2(1-k_1)}$
2.1	$1 < \beta \le \alpha$ $0 < \lambda \le \infty$	$k_{21} = \frac{D_{21} - \sqrt{D_{21}\gamma\beta^2}}{D_{21} - \gamma\beta^2}$ $D_{21} = \eta\left(\beta^2 - 2\beta + 1\right) + 2\beta - 1$	$M'_{21} = \frac{\left(2\gamma\beta^3 - C_{21}\right)k_{21}^3 + 3C_{21}k_{21}^2 - 3C_{21}k_{21} + C_{21}}{1-k_{21}}$ $C_{21} = \frac{(2\beta^3 - 3\beta^2 + 1)\eta + 3\beta^2 - 1}{\beta^2}$	$\phi'_{21} = \frac{\beta}{2(1-k_{21})}$
2.2	$1 < \beta \le \alpha$ $\infty < \lambda \le \lambda_{cu}$	$k_{22} = \frac{D_{22}}{D_{22} + 2\omega\gamma\beta}$, $D_{22} = D_{21} + \gamma\omega^2$	$M'_{22} = \left(3\gamma\omega\beta^2 + C_{22}\right)k_{22}^2 - 2C_{22}k_{22} + C_{22}$, $C_{22} = C_{21} - \frac{\gamma\omega^3}{\beta^2}$	$\phi'_{22} = \frac{\beta}{2(1-k_{22})}$
3.1	$\alpha < \beta \le \beta_{tu}$ $0 < \lambda \le \infty$	$k_{31} = \frac{D_{31} - \sqrt{D_{31}\gamma\beta^2}}{D_{31} - \gamma\beta^2}$ $D_{31} = \eta\left(\alpha^2 - 2\alpha + 1\right) + 2\mu(\beta - \alpha) + 2\alpha - 1$	$M'_{31} = \frac{\left(2\gamma\beta^3 - C_{31}\right)k_{31}^3 + 3C_{31}k_{31}^2 - 3C_{31}k_{31} + C_{31}}{1-k_{31}}$ $C_{31} = \frac{(2\alpha^3 - 3\alpha^2 + 1)\eta - 3\mu\left(\alpha^2 - \beta^2\right) + 3\alpha^2 - 1}{\beta^2}$	$\phi'_{31} = \frac{\beta}{2(1-k_{31})}$
3.2	$\alpha < \beta \le \beta_{tu}$ $\infty < \lambda \le \lambda_{cu}$	$k_{32} = \frac{D_{32}}{D_{32} + 2\omega\gamma\beta}$, $D_{32} = D_{31} + \gamma\omega^2$	$M'_{32} = \left(3\gamma\omega\beta^2 + C_{32}\right)k_{32}^2 - 2C_{32}k_{32} + C_{32}$, $C_{32} = C_{31} - \frac{\gamma\omega^3}{\beta^2}$	$\phi'_{32} = \frac{\beta}{2(1-k_{32})}$

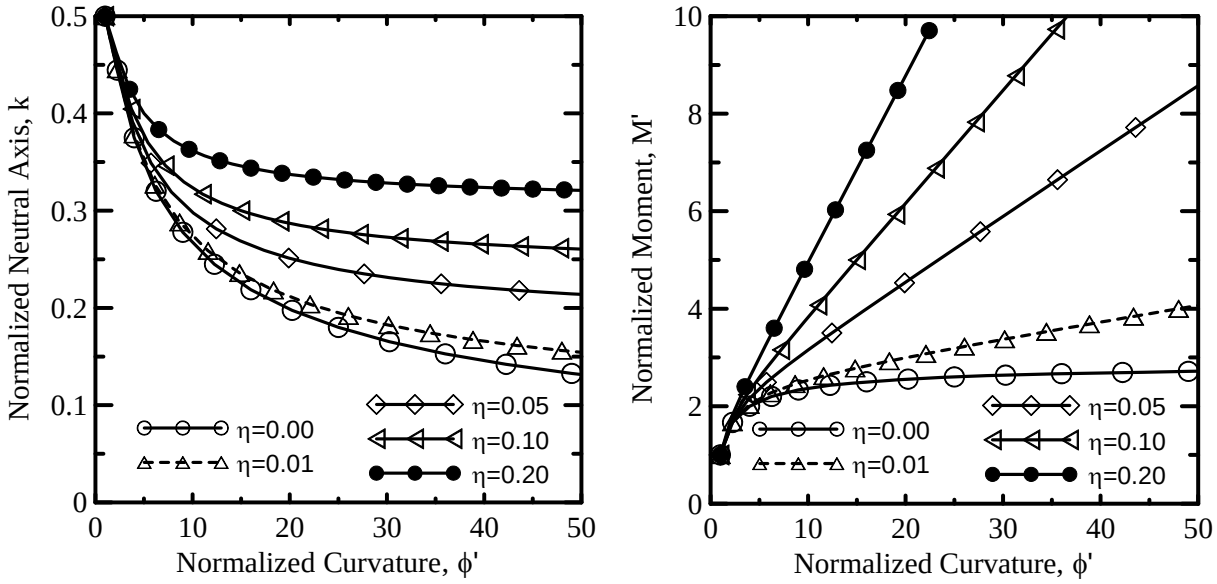

Fig. 3: Effect of a) Depth of Neutral axis on the Moment capacity of a section, and b) the moment curvature response in the Range 2.1

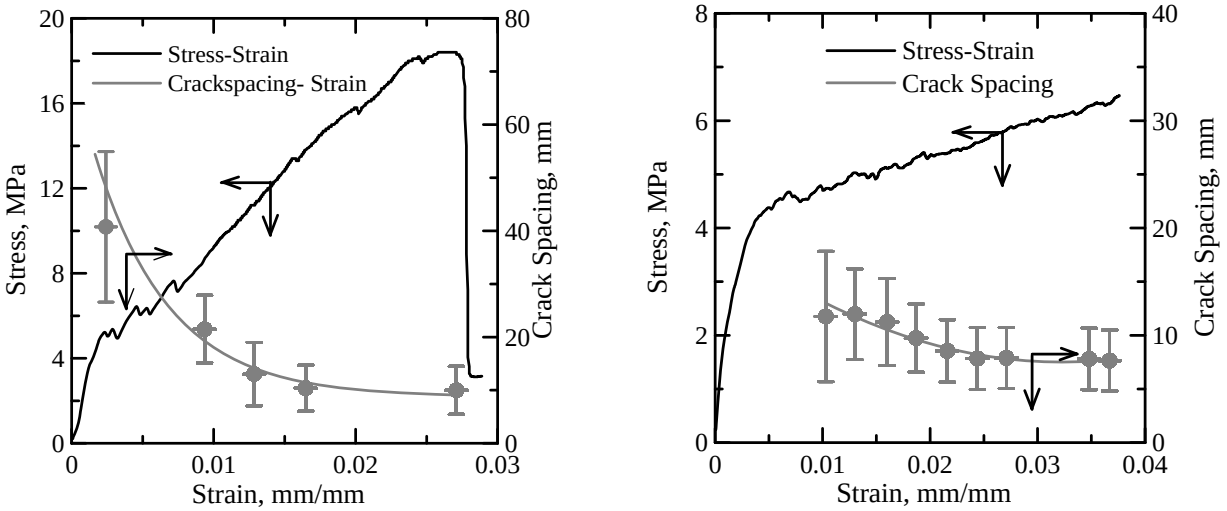

Fig. 4: Uniaxial tension stress strain response of a) AR-Glass and b) Polyethylene fabric composites.

In order to correlate the tension and bending responses, the simulation procedure employed experimental data from a set of specimens under uniaxial tension and three point bending tests. Tension specimens were approximately 10x25x200 mm. Flexural specimens for the four point bending test were 10x25x200 mm with a clear span of 152 mm. Fig. 5(a) shows the tension test results of a specimen along with the fitted tension model that is used in simulation. No attempt was made to obtain a best fit curve to the response. The parameters for the bilinear tension model were obtained by fitting the model to uniaxial tension test results. The

material properties for the simulation of AR Glass Fabric composites were : α= 100, μ = 0.1, η = 0.05, γ = 1.0, and, ω = 20.4, while the limits of the modeling were β_{tu} = 250, and λ_{cu} = 150. The Young modulus of tension and compression response (*E*) was obtained by assuming a value of 18000 MPa, and a first crack strain capacity of ε_{cr} = 0.0002 was used. The ultimate strain capacity was computed from the overall response. One can also conduct a back-calculation procedure of the load deflection curve to obtain the initial modulus of the tensile response *E* directly from the uniaxial test. The ultimate compressive strength of cement pastes was assumed to be the typical value of f'_{cr}= Eω ε_{cr} = 20.4(18)(0.0002)= 73.4 MPa.

Figure 5b shows the predicted flexural load deflection response of cement composites. The steps in calculation of load-defelection response form the moment-curvature have been discussed in detail in recent publications dealing with strain hardening [10] and strain softening type composites [11][12]. Note that in these systems, the high tensile stiffness and strength of the composite leads to high values for the load, and distributed flexural cracking. Analysis of the samples indicates formation of diagonal tensions cracks in the samples due to the shear failure mechanism. No provisions for shear cracking were accounted in for the present approach. No attempt was made to simulate the response beyond the first major flexural crack.

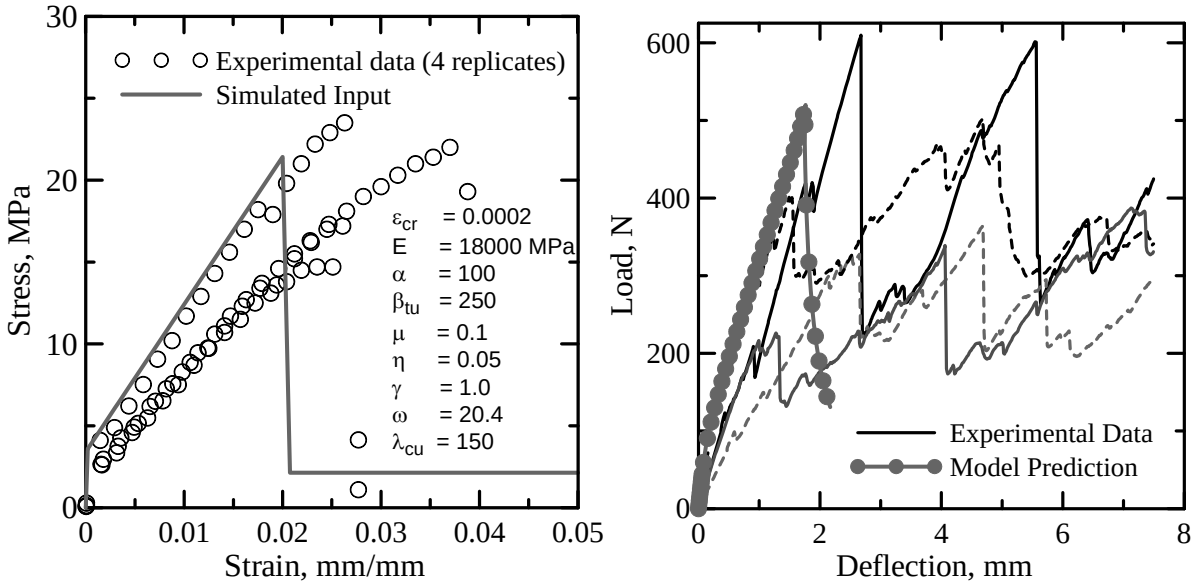

Fig. 5: Tensile stress strain response input model and predicted load deflection response of AR-Glass fabric composites.

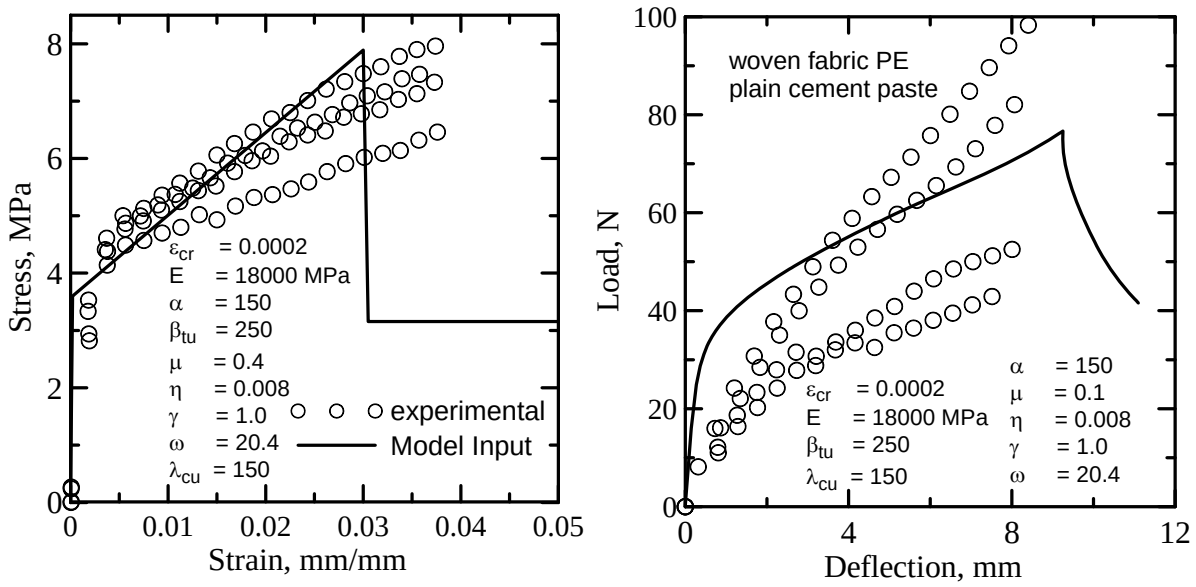

Fig. 6: Tension stress strain response input model and predicted load deflection response of Polyethylene (PE) fabric composites.

The material properties for the simulation of PE fabric composites were: $\alpha = 150$, $\mu = 0.4$, $\eta = 0.008$, $\gamma = 1.0$, and, $\omega = 20.4$. the constants were $\varepsilon_{cr} = 0.0002$, and E = 18000 MPa, while the limits of the modeling were $\beta_{tu} = 250$, and $\lambda_{cu} = 150$. The overall tensile response for the PE composites is shown in Figure 6.a.

To demonstrate the ability of the algorithm to predict load-deflection response for strain hardening material, the flexural specimens for the four point bending test were 25 x 10 x 200 mm with a clear span of 152 mm. The material parameters for tension model were determined by fitting the model to the uniaxial tension test result as shown by the solid line in Fig. 5(a) and 6(a). The average material properties were: compressive strength f_c' = 73.4 MPa. The initial tensile modulus E = 18 GPa and the first cracking tensile strain ε_{cr} = 200 μstr were used as they correlated with the uniaxial tensile test results. The ultimate compressive strain ε_{cu} was assumed to be $\alpha\, \varepsilon_{cr}$ = 150 (0.0002) = 3%. All parameters used in the simulation are provided in the same figure. The solid curves in Fig. 5(b) and 6(b) show the predicted flexural response obtained by the simulation process. The prediction for the strain hardening material during the pre- and post-crack stages agreed well with the experimental results; Note that the formation of the distributed crack system can be adequately described by the smeared pseudo-strain model.

Figures 5 (b) and 6 (b) show the predictions of the equivalent load-deflection response for AR glass and PE fabrics respectively. Simulation using direct tension data underestimates the equivalent flexural stress. This may be due to several factors including the size effect, uniformity in loading in tension vs. the linear strain distribution in flexure. The underestimation of the flexural capacity of the beam can be eliminated by increasing the tensile capacity by a scaling parameters as discussed in earlier publications, however these topics are beyond the

scope of present work. Alternatively, one can use the flexural response and develop a back-calculation procedure to calculate a direct fit to the experimental flexural data.

5 Design Example- Simply supported Beam Under Distributed Load

The methodology used in the design of conventional reinforced concrete according to ACI-318 [13] is adopted next. The nominal moment capacity of a flexural member M_n must be decreased by a reduction factor to account for variability in materials and workmanships. The reduced capacity must be greater than the ultimate moment M_u due to factored loading by ACI Sec. 9.2.

$$\phi_r M_n \geq M_u \tag{13}$$

where ϕ_r is the reduction factor for strain-hardening FRC and may be conservatively taken as 0.65, equal to the reduction factor for compressive failure of plain concrete as stipulated by ACI Sec. C.3.5. Despite the post-crack flexural response of HPFRC is ductile such that it can sustain large deflections after cracking, it fails abruptly with little warning after passing the ultimate moment. For this reason, a conservative reduction factor for compressive failure of plain concrete is adopted. Equations 7 and 8 derived earlier in addition to the parameters of Table 2, form the basis for the design procedures.

The objective of this section is to design a 300 mm span simply supported beam subjected to a uniformly distributed live load pressure of 550 kPa. The material is a strain-hardening GFRC with Young's modulus E =15 GPa, cracking tensile strength σ_{cr} of 5.85 MPa, and an ultimate compressive strength f_c' of 65 MPa. The ultimate tensile strength σ_{peak} of 9 MPa, tensile strain at peak strength ε_{peak} of 0.009 and density of 20.4 kN/m^3 are used.

While the self weight is negligible compared to the load applied, however in this case it is computed to illustrate the factored loads. By assuming a thickness between 100 and 150 mm, one can calculate the self weight as:

$$w_{sw} = 0.15 \times 20.4 = 3.06 \text{ kPa}$$

The ultimate factored load is calculated as:

$$w_u = 1.2(DL) + 1.6(LL) = 1.2(3.06) + 1.6(550) = 884 \text{ kPa}$$

Consider the beam over a strip one meter in width one can calculate the maximum moment at mid span of the beam as the design load:

$$M_u = \frac{w_u L^2}{8} = \frac{884 \times 0.3^2}{8} = 9.94 \text{ kN-m/m}$$

The next step is to calculate the normalized moment capacity of the GFRC used in this design which requires calculation of the material parameters according to Eqs. (1) – (4) as follows:

Cracking tensile strain, $\varepsilon_{cr} = \frac{\sigma_{cr}}{E} = \frac{5.85}{15000} = 3.9\times10^{-4}$

Normalized tensile strain at peak strength, $\alpha = \frac{\varepsilon_{peak}}{\varepsilon_{cr}} = \frac{0.009}{3.9\times10^{-4}} = 23.1$

Normalized post-crack tensile modulus, $\eta = \frac{E_{cr}}{E} = \frac{9-5.85}{(0.009-0.00039)\times15000} = 0.0244$

Normalized yield compressive strain, $\omega = \frac{\sigma_{cy}}{\sigma_{cr}} = \frac{0.85\times f_c^{'}}{\sigma_{cr}} = \frac{0.85\times65}{5.85} = 9.4$

The neutral axis and normalized moment capacity can be calculated by using the maximum value of $\beta = \alpha$ in Eqs. (8)&(10) as the ultimate tensile capacity:

$$C_1 = \eta\left(\beta^2 - 2\beta + 1\right) + 2\beta - 1 = 0.0244\left(23.1^2 - 2\times23.1 + 1\right) + 2\times23.1 - 1 = 57.12$$

Neutral axis depth parameter, $k = \frac{C_1 - \sqrt{\beta^2 C_1}}{C_1 - \beta^2} = \frac{57.12 - \sqrt{23.1^2\times57.12}}{57.12 - 23.1^2} = 0.246$

$$C_2 = C_1 + 2C_1\beta - \beta^2 = 57.12 + 2\times57.12\times23.1 - 23.1^2 = 2162$$

Therefore the normalized moment capacity is obtained as:

$$m_n = C_2\frac{k^2 - 2k + 1}{\beta^2} + \frac{2\beta k^3}{1-k} = 2162\frac{0.246^2 - 2\times0.246 + 1}{23.1^2} + \frac{2\times23.1\times0.246^3}{1-0.246} = 3.21$$

At this stage one has to verify that the normalized compressive strain developed at the top fiber by Eq. (10).

$$\lambda = \frac{k}{1-k}\beta = \frac{0.246}{1-0.246}23.1 = 7.54 < \omega = 9.5 \quad \text{=>OK}$$

The compressive strain is in the elastic stage; therefore the calculated normalized moment m_n = 3.21 is valid. By using the normalized moment capacity, one can determine the cracking moment required to carry the ultimate moment by Eqs. (6), (7),&(8).

$$M_{cr} = \frac{M_n}{m_n} = \frac{M_u}{\phi_r m_n} = \frac{9.94}{0.65\times3.21} = 4.76 \text{ kN-m/m}$$

Finally, the required thickness is determined by Eq. (7)

$$h = \sqrt{\frac{6M_{cr}}{\sigma_{cr}b}} = \sqrt{\frac{6\times4760}{5.85\times10^6\times1}} = 0.07 \ m$$

At this stage, one can use a thickness of 75 mm which is less than the assumed thickness of 150 mm in the estimation of the self weight (conservative). It is not necessary to recalculate the new self weight since the weight is negligible compared to the live load.

Alternatively, one can use the design charts presented in Fig. 7 can be used to quickly estimate the normalized moment capacity. The use of the chart requires one to first draw a vertical line from $\beta = \alpha = 23.1$ to the curve at $\eta = 0.0244$, and get $m_n = 3.25$ from the m_n - β chart. This establishes the normalized moment capacity. In order to check for the range of applicability of the equation, one has to continue the vertical line and get $\lambda = 7.7$ from the λ - β chart. Since λ is lower than the normalized yield compressive strain $\omega = 9.4$, the assumption of failure in the elastic compression zone and the obtained value of $m_n = 3.25$ is valid. It can be seen that the values $\lambda = 7.7$ and $m_n = 3.25$ manually picked from the charts are very close to the exact values $\lambda = 7.54$ and $m_n = 3.21$ directly computed from the equations. Once m_n is identified, the required cracking moment M_{cr} and thickness h can be calculated using an elastically equivalent section as shown before.

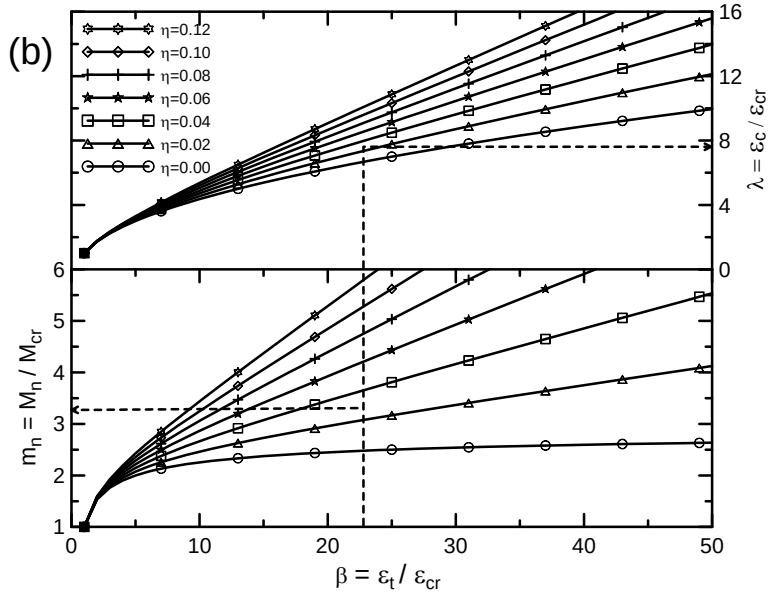

Fig. 7: Design Chart for the three point beam design using the closed form equations

6 References

1] NAAMAN A.E.; REINHARDT H.W.; *Setting the stage: toward performance based classification of FRC composites*, In: Proc of 4th Int workshop on High Performance Fiber Reinforced Cement Composites (HPFRCC-4), Ann Arbor, USA, June 15-18, 2003, p. 1–4.

[2] LI V.C.; *From micromechanics to structural engineering – the design of cementitious composites for civil engineering applications*, Struct Eng Earthquake Eng, 1994; 10(2): 1–34.

[3] BENSON S.D.P.; KARIHALOO B.L.; *CARDIFRC® - Development and mechanical properties. Part III: Uniaxial tensile response and other mechanical properties*, Magazine of Concrete Research, 2005;57(8):433-443.

[4] CHANVILLARD, G.; RIGAUD, S.; *Complete characterization of tensile properties of Ductal UHPFRC according to the French recommendations*, 4th Int RILEM workshop, High Performance Fiber Reinforced Cement Composites (HPFRCC4), Ann Arbor, USA, June 15-18, 2003, p. 21-34.

[5] LI, V. C.; *On engineered cementitious composites (ECC), A review of the material and its applications.* Journal of Adv. Concrete Technology, 2003;1(3):215-230.

[6] NAAMAN A.E.; REINHARDT H.W.; *Proposed classification of HPFRC composites based on their tensile response.* Mater Struct, 2006;39(289):547–555.

[7] SORANAKOM C; MOBASHER B.; *Correlation of tensile and flexural response of strain softening and strain hardening cement composites*, Cement and Concrete Composites, 2008;30:465-477.

[8] PELED A.; MOBASHER, B.; *Pultruded fabric-cement composites*, ACI Materials Journal 2005;102(1):15-23.

[9] MOBASHER B.; PELED A,; PAHILAJANI J.; *Distributed cracking and stiffness degradation in fabric-cement composites*, Materials and Structures 2006; 39(287):317–331.

[10] SORANAKOM C.; MOBASHER B.; "*Closed-form moment-curvature expressions for homogenized fiber reinforced concrete*, " ACI Material Journal, 2007; 104(4):351-9.

[11] SORANAKOM, C.; MOBASHER. B.; BANSAL S.; "*Effect of material non-linearity on the flexural response of fiber reinforced concrete*," Proceeding of the Eighth International Symposium on Brittle Matrix Composites BMC8, Warsaw, Poland, 2006:85-98.

[12] SORANAKOM, C.; MOBASHER B.; "*Closed form solutions for flexural response of fiber reinforced concrete beams,*" Journal of Engineering Mechanics, 2007;133(8):933-41.

[13] ACI COMMITTEE 318; *Building Code Requirements for Structural Concrete*. ACI Manual of Concrete Practice, American Institute, Detroit, USA, 2005.